RSC
Sustainability

ROYAL SOCIETY
OF CHEMISTRY

PAPER

View Article Online
View Journal | View Issue

Photocatalytic and antimicrobial polymer-based hybrid membranes with surface-modified TiO_2 nanoparticles with 5-aminosalicylic acid and silver nanoparticles

Joana M. Queirós,[abc] Fangyuan Zheng,[bcg] Ricardo Brito-Pereira,[g] Margarida M. Fernandes,[acde] Estela O. Carvalho,[ac] Pedro M. Martins,*[bc] Vesna Lazić,*[f] Jovan M. Nedeljković[f] and Senentxu Lanceros-Mendez[agh]

The sustainability of water treatment is a growing environmental and public health concern, particularly regarding the removal of antibiotics and microorganisms. This study developed multifunctional membranes using synthetic (PVDF-HFP) and natural (silk fibroin, SF) polymer matrices incorporating TiO_2 nanoparticles surface-modified with 5-aminosalicylic acid (5-ASA) and silver (Ag). These modifications enhanced both visible-light-responsive photocatalytic activity and antimicrobial performance. The membranes were evaluated for ciprofloxacin degradation and antimicrobial activity against Gram-positive and Gram-negative bacteria. Photocatalytic PVDF-HFP membranes achieved 63% and 62% under UV and simulated solar radiation, respectively, while SF membranes reached 50% and 71%. Antimicrobial efficiency showed a $\sim$2 $\log_{10}$ bacterial reduction for *E. coli* and a 0.5 $\log_{10}$ reduction for *S. epidermidis*, attributed to the presence of Ag in the TiO_2/5-ASA nanoparticles. Furthermore, the membranes maintained stable performance across multiple reuse cycles. Overall, the results highlight the potential of these multifunctional materials as efficient and eco-friendly solutions for advanced wastewater treatment applications.

Check for updates

Cite this: *RSC Sustainability*, 2025, **3**, 4568

Received 4th July 2025
Accepted 6th August 2025

DOI: 10.1039/d5su00569h

rsc.li/rscsus

Sustainability spotlight

This work highlights the sustainable development of photocatalytic membranes through the green synthesis of Ag–TiO_2 nanoparticles and their immobilisation into a natural biopolymer, silk fibroin, aligning with the UN's Sustainable Development Goals, particularly Goal 6 (Clean Water and Sanitation) and Goal 12 (Responsible Consumption and Production). By combining a natural polymer with greener photocatalysts, this approach reduces environmental impact and energy consumption, offering a sustainable alternative to conventional synthetic membranes based on PVDF-HFP. These materials present high photocatalytic efficiency in degrading ciprofloxacin under UV and simulated solar irradiation over various cycles and antimicrobial properties, offering an innovative, eco-friendly, and efficient solution for degrading the persistent water pollutants, mitigating the antibiotic resistance risk and supporting the sustainable management of contaminated water.

1 Introduction

Water pollution is one of Humankind's most critical challenges,[1,2] contributing to nearly 1.5 million deaths yearly due to the consumption of unsafe water.[3] In recognition of this, ensuring access to clean water and sanitation was established as the sixth goal of the United Nations Sustainable Development Goals (SDGs).[4–6]

Among water contaminants, contaminants of emerging concern (CECs)[7–9] have received growing attention due to their frequent detection in aquatic ecosystems at low concentrations (ng L^{-1} to μg L^{-1}).[10,11] Pharmaceuticals constitute one of the largest groups of CECs, gaining prevalence due to their wide use to treat various diseases and areas that are persistent in water bodies.[12–14] Antibiotics are especially concerning, as they have

---

[a] Physics Centre of Minho and Porto Universities (CF-UM-UP) and LaPMET - Laboratory of Physics for Materials and Emergent Technologies, University of Minho, Braga, 4710-057, Portugal
[b] Centre of Molecular and Environmental Biology, University of Minho, Braga, 4710-057, Portugal. E-mail: pamartins@bio.uminho.pt
[c] IB-S – Institute for Research and Innovation on Bio-Sustainability, University of Minho, Portugal
[d] CMEMS UMinho, University of Minho, Guimarães 4800-058, Portugal
[e] LABBELS – Associate Laboratory, Guimarães 4800-058, Portugal
[f] Vinča Institute of Nuclear Sciences – National Institute of the Republic of Serbia, University of Belgrade, Centre of Excellence for Photoconversion, PO Box 522, 11001 Belgrade, Serbia. E-mail: vesna.lazic@vin.bg.ac.rs
[g] BCMaterials, Basque Centre for Materials, Applications and Nanostructures, UPV/EHU Science Park, 48940 Leioa, Spain
[h] Ikerbasque, Basque Foundation for Science, 48009 Bilbao, Spain

been detected in various types of water matrices worldwide, including groundwater and drinking water.[15,16]

Quinolones, such as ofloxacin, ciprofloxacin, and norfloxacin, are extensively used in the treatment of human and animal infections.[17,18] A substantial portion of these drugs remains unmetabolised and is excreted through urine and faeces, entering wastewater systems.[19,20] Ciprofloxacin (CIP) is a widely prescribed and valued for its broad efficacy and cost-effectiveness.[21] However, its incomplete removal in conventional wastewater treatment plants (WWTPs) contributes to its environmental dissemination. CIP exposure has been associated with health risks including altered intestinal microflora, increased susceptibility to infections, and potential carcinogenic effects.[22–24] Moreover, the release of antibiotics into the environment promotes the development of antimicrobial resistance in microorganisms, facilitating the occurrence of antibiotic-resistant bacteria (ARB).[25–27] This reduces the effectiveness of antibiotics in treating bacterial infections.[28] For instance, some studies have shown that CIP concentrations as low as 0.1 $\mu g\ mL^{-1}$ in drinking water can induce resistance in *Staphylococcus aureus*, *Pseudomonas* sp., and *Enterococcus* sp.[28,29]

In this context, the development of materials capable of degrading persistent antibiotics and simultaneously presenting antimicrobial properties is urgently needed.

Photocatalytic nanomaterials have received considerable attention in water remediation for CEC degradation and application against ARB.[11,30–32] An effective strategy for extending the photocatalytic activity of wide band gap oxides, such as titanium dioxide (TiO_2) nanoparticles (NP), into the visible range is to form an Interfacial Charge Transfer (ICT) complex with organic ligands.[33,34] These hybrids can be formed by coordinating salicylate-type ligands such as 5-aminosalicylic acid (5-ASA), an anti-inflammatory drug known as mesalazine, to the surface Ti atom. Furthermore, introducing noble metals, such as Ag, improves charge separation[35,36] and endows antimicrobial activity.[37]

Despite the efficiency of the photocatalytic nanoparticles, a more cost-effective process that allows reusability and prevents possible secondary pollution (release of NP into water into water bodies),[38–41] can be developed by immobilising them in polymeric matrices. Polymers are widely used as nanoparticle support materials since they are inexpensive, flexible, thermal, chemical, and mechanically stable.[42,43] Among them, synthetic polymers poly(vinylidene fluoride) (PVDF) and its copolymers, including poly (vinylidene fluoride-*co*-hexafluoropropylene) (PVDF-HFP)[44] have been extensively used as membrane materials for water remediation applications[45–47] due to their mechanical robustness, UV resistance, and compatibility with various processing technologies.[46–49] Nevertheless, PVDF-HFP is derived from non-renewable[50] fossil resources and is resistant to natural degradation,[51] raising concerns about the potential release of toxic compounds and microplastics,[51,52] which could have long-term environmental impacts.[53–55] Additionally, its processing is commonly associated with the use of toxic solvents (*e.g.*, dimethyl formamide (DMF)).[50,52]

Though synthetic polymers are still the best option for high-performance applications. Regarding other applications, it is possible to focus on alternatives based in green chemistry and circular economy paradigms, developing sustainable materials[56–59] to address climate change.[51,56] In this context, natural polymers, such as cellulose,[56] chitosan,[60] and silk,[61] arise as a potential solution, as they are biodegradable and are produced from renewable sources such as plants, animals, and microbes.[51,62,63]

Among them, silk obtained from the *Bombyx mori* silkworm has attracted much attention.[64–66] Silk fibroin (SF), the main structural protein of silk,[67,68] is composed of α-helices, β-sheet crystal structure and random coils assembled by repetitive amino acid sequences.[67,69] SF also presents biocompatibility, flexibility, and stability in most organic solvents and water, making it a good candidate for environmentally friendly materials development.[67,68,70,71] Moreover, SF, similarly to PVDF, can be processed into different morphologies, such as film[72] 3D porous scaffolds and membranes,[73] electrospinning,[74] spin coating,[72] salt-leaching,[73] among others. Thus, SF-based materials have been used in biomedical, electronic, sensing, optical applications, and water remediation.[75–79]

Combining the activity of green functionalised photocatalysts with visible spectral range activity and antimicrobial effects incorporated into a natural polymer matrix presents a novel alternative to conventional PVDF-based membranes. The resulting hybrid materials may offer performance comparable to fossil-based polymers while significantly reducing environmental impact. This approach aligns with sustainable development goals and represents a step forward in advanced water treatment technologies.

In this study, TiO_2 nanoparticles were functionalised with Ag nanoparticles using 5-aminosalicylic acid as a green methodology. Afterwards, the nanocomposite particles were incorporated into PVDF-HFP and SF polymer matrices. The resulting membranes were tested for their photocatalytic efficiency in degrading ciprofloxacin, their antibacterial properties against Gram-positive and Gram-negative bacteria, as well as their reusability in cycling experiments. This work aims to validate the green transition from synthetic to natural polymer in the development of multifunctional membranes for the sustainable treatment of contaminated water.

2 Materials and methods

2.1 Materials

Bombyx mori silkworm cocoons were supplied by APPACDM from Castelo Branco (Portugal). Sodium carbonate (Na_2CO_3), formic acid (FA, CH_2O_2), calcium chloride ($CaCl_2$) and sodium chloride (NaCl) were sourced from Sigma-Aldrich. Distilled water was prepared on-site in the laboratory. Poly(vinylidene fluoride-*co*-hexafluoropropylene) (PVDF-HFP, SOLEF®) was obtained from Solvay, while Fischer-Scientific supplied *N*,*N*-dimethylformamide (DMF, ≥99%). Ciprofloxacin ($C_{17}H_{18}FN_3O_3$) was purchased from Sigma-Aldrich. Silver nitrate ($AgNO_3$) was acquired from VWR, and 5-aminosalicylic acid from Alfa Aesar. All chemicals and solvents were used without further purification.

2.2 Synthesis and characterisation of nanoparticles

The surface functionalisation of TiO_2 nanoparticles (Degussa P-25, with a specific surface area (BET) of 35–65 $m^2\ g^{-1}$) with 5-ASA was carried out according to the procedure described in.[80] In brief, 100 mg of TiO_2 nanoparticles were dispersed in 30 mL of deionised water containing 30.6 mg 5-ASA and stirred overnight. The change in the nanoparticles' colour evidences the successful formation of the ICT complex. Afterwards, the modified TiO_2 nanoparticles were separated *via* centrifugation, thoroughly rinsed with water five times, and vacuum-dried at 40 °C in a GCA Corporation, USA, oven.

A nanocomposite of Ag NPs on the surface of TiO_2 nanoparticles functionalised with 5-ASA was synthesised by utilising the reducing properties of the free amino groups in 5-ASA molecules.[81] Specifically, 200 mg of surface-modified TiO_2 with 5-ASA was mixed with 20 mg of $AgNO_3$ in 50 mL of Ar-saturated water, and the mixture was refluxed at 60 °C for 6 hours under continuous stirring. The resulting nanocomposite was isolated by centrifugation, repeatedly washed with water, and dried under vacuum at 40 °C in a GCA Corporation oven. For simplicity, the surface-modified TiO_2 with 5-ASA and the nanocomposite consisting of Ag NPs supported on TiO_2 with 5-ASA will be referred to as TiO_2/5-ASA and TiO_2/5-ASA/Ag, respectively.

The TiO_2/5-ASA/Ag nanocomposite composition, including silver and titanium content, was quantified using inductively coupled plasma optical emission spectroscopy (ICP-OES Thermo Scientific iCAP 7400). Transmission electron microscopy (TEM) imaging was performed using a JEOL JEM-2100 LaB_6 instrument operated at 200 kV, with images acquired using a Gatan Orius CCD camera set to 2× binning. X-ray diffraction (XRD) was carried out using a Rigaku SmartLab system with Cu $K\alpha_{1,2}$ radiation, employing a continuous angular scanning rate at 2° min^{-1}. Reflectance spectra of TiO_2/5-ASA and TiO_2/5-ASA/Ag samples were measured using a Shimadzu UV-Visible UV-2600 spectrophotometer equipped with an integrated sphere ISR-2600 Plus.

2.3 Extraction of SF

The extraction of SF from *Bombyx mori* silkworm cocoons was performed using a soap degumming method.[82] The cocoons were cleaned, cut into 2 cm^2 pieces, and boiled in a 0.05 wt% Na_2CO_3 solution for 30 min, maintaining an SF-to-water solution ratio (w/v) of 1 : 40. The resultant fibres of SF underwent extensive rinsing with distilled water before being air-dried at room temperature for 24 hours. These fibres were dissolved in a 0.19 M FA/$CaCl_2$ solution in a 10 : 1 v/w ratio (FA : SF). Impurities were removed by centrifugation (Hettich EBA 21) at 6000 rpm for 10 min, and the supernatant SF/FA/$CaCl_2$ solution was filtered. The filtered solution was then cast onto a Petri dish and allowed to dry at room temperature for 24 hours for FA evaporation. The final transparent, plastic-like material was rinsed in a distilled water bath to eliminate residual $CaCl_2$ and air-dried at room temperature for 24 hours, resulting in a brittle, whitish solid form of SF.

2.4 Development of polymer-based porous membranes

The synthesised nanoparticles TiO_2/5-ASA and TiO_2/5-ASA/Ag were immobilised into a PVDF-HFP and silk-based membrane by temperature-induced phase separation (TIPS) combined with salt leaching techniques. This combination of methods allows greater control over the pore size range and promotes enhanced pore interconnectivity.[83] For the preparation of the PVDF-HFP-based membranes, TiO_2/5-ASA and TiO_2/5-ASA/Ag nanoparticles were first dispersed in 9 mL of DMF in an ultrasonication bath for 2 h to achieve good nanoparticle dispersion. Afterwards, 1 g of PVDF-HFP polymer was added to the solution to obtain PVDF-HFP : TiO_2/5-ASA and PVDF-HFP : TiO_2/5-ASA/Ag with a final mass ratio of 10 : 1, a concentration reported as ideal for obtaining high degradation efficiency without compromising the remaining physical–chemical properties of the polymer.[11] Pristine membranes were also prepared and identified as PVDF-HFP. The solution was mechanically agitated until the polymer was completely dissolved. At this stage, 9 g of NaCl, previously sieved (100 μm mesh), was added to the solution and stirred until a homogeneous and viscous solution was obtained. The nanoparticle/polymer/salt solution was poured into a Petri dish. The DMF was evaporated at room temperature for nearly one week until complete solvent evaporation. When the membranes were dried entirely, they were submerged under agitation to allow the NaCl to leach for 5 days, changing the water frequently. Electrical conductivity measurements were performed on the water solution to confirm constant values, indicating that NaCl had been completely removed from the polymer microstructure (Fig. 1).

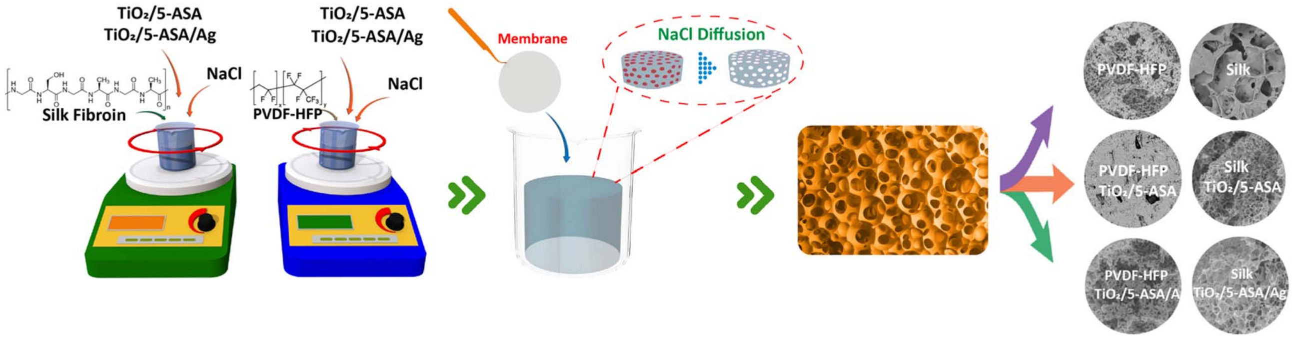

Fig. 1 Schematic representation of the methodology to develop the PVDF-HFP- and SF-based pristine and nanocomposite membranes.

To produce SF membranes, the TiO_2/5-ASA and TiO_2/5-ASA/Ag nanoparticles were dispersed in 10 mL of FA in an ultrasonication bath for 2 h to achieve good nanoparticle dispersion. Subsequently, 1 g of SF was added to obtain a 10 : 1 v/w FA : SF solution. The solution was mechanically agitated for 1 h to ensure complete dissolution. SF (pristine membranes) were also developed. At this point, 9 g of NaCl, sifted through a 100 μm mesh, was incorporated into the solution and agitated until a uniform and viscous solution was achieved. Then, the nanoparticles/polymer/salt solution was placed in a Petri dish and left to dry for 24 hours to evaporate the solvent fully. These membranes were designated SF, SF : TiO_2/5-ASA, and SF : TiO_2/5-ASA/Ag. Similar to the PVDF-HFP membranes, the SF-based membranes were submerged in water under agitation to allow the NaCl to leach for 5 days, changing the water frequently. The porous membranes were then obtained and dried in an airing chamber (Christ Beta 2–8 LDplus) for 24 h. The preparation procedure of the membranes is summarised in Fig. 1.

2.5 Polymer-based membranes' physical-chemical characterisation

Fourier-transform infrared spectroscopy (FTIR) measurements for PVDF-HFP-based and SF-based membranes were conducted at room temperature using a Jasco FT/IR-6100 spectrometer. The infrared spectra range from 600 to 4000 cm^{-1}, employing 32 scans with a resolution of 4 cm^{-1}. To assess the relative content of the secondary structures present in each SF-based sample, the amide I spectral regions were deconvolved using OriginPro 8.1 software (OriginLab, Northampton). The analysis included linear baseline correction with the Savitzky–Golay method, using 15 points. Peak positions and component numbers identified *via* the second derivative served as initial parameters for iterative curve fitting using a Gaussian function using the Levenberg–Marquardt algorithm ($R^2 > 0.999$).[84] Curve fitting was applied uniformly across all samples to ensure comparable secondary structure assignments. The relative contribution of each fitted component to the amide I band was calculated by integrating the area under the curve and normalising it to the total amide I area.

The β-phase relative fraction, $F(\beta)$, of the PVDF-HFP-based membranes was calculated using eqn (1):

$$F(\beta) = \frac{A_\beta}{\left(\frac{K_\beta}{K_\alpha}\right)A_\alpha + A_\beta} \tag{1}$$

where A_α and A_β represent absorbances at 766 and 840 cm^{-1}, respectively, and K_α (6.1×10^4 cm^2 mol^{-1}) and K_β (7.7×10^4 cm^2 mol^{-1}) are the corresponding absorption coefficients.[3,85]

Differential scanning calorimetric (DSC) measurements were performed in a Mettler Toledo DSC 822e. For PVDF-HFP-based membranes, the samples were heated from 25 °C to 200 °C. SF-based membranes were heated from 25 °C to 170 °C before being cooled back to 25 °C to eliminate absorbed water. Subsequently, they were reheated from 25 °C to 350 °C. All the heating and cooling processes were performed at 10 °C min^{-1} under a nitrogen atmosphere (flow rate, 20 mL min^{-1}) in aluminium pans with perforated lids to facilitate the release and removal of volatiles. The degree of crystallinity of the PVDF-HFP-based membranes was calculated using eqn (2):

$$\chi_c = \frac{\Delta H_f}{x\Delta H_\alpha + y\Delta H_\beta} \tag{2}$$

where ΔH_f denotes the melting enthalpy of the PVDF-HFP polymer from the DSC analysis, and x and y are the α and β-phase contents, respectively, obtained from the FTIR spectra. ΔH_α and ΔH_β are the melting enthalpies of pure crystalline α-PVDF (93.04 J g^{-1}) and β-PVDF (103.40 J g^{-1}) samples, respectively.[86]

2.6 Polymer-based membranes' functional performance

2.6.1 Polymer-based membranes' photocatalytic activity. To evaluate the photoactive performance of the nanocomposite membranes, ciprofloxacin (CIP) was used as an organic compound to monitor the degradation under ultraviolet (UV) and simulated solar radiation (VIS). Photocatalytic tests were conducted using a 5 cm × 3 cm membrane sample, affixed to the inner wall of a beaker containing 50 mL of CIP solution (C_0 = 5 mg L^{-1}, pH = 2.9) and stirred for 30 minutes in the absence of light (dark). After this period, all the samples were exposed to eight 8 W UV lamps (PHILIPS TL 8 W BLS, Poland) with a peak emission at 385 nm over 600 min. The distance between the solution and the lamp was 13.5 cm, with an irradiance at the sample of 3.3 W m^{-2}. Similarly, the PVDF-HFP, PVDF-HFP: TiO_2/5-ASA/Ag, SF and SF : TiO_2/5-ASA/Ag membranes were evaluated under simulated solar radiation using a Xenon lamp with a peak emission at 550 nm and an irradiance of 300 W m^{-2}, also over 600 min. In this case, the lamp was positioned 21 cm away from the solution. The photocatalytic degradation efficiencies of CIP were monitored by measuring the variation of its maximum absorption peak at 277 nm at specific time intervals using an Infinite M Plex spectrophotometer (TECAN). The pollutant concentration over time was determined using eqn (3):

$$\eta\% = \frac{C_0 - C}{C_0} \times 100 \tag{3}$$

where C_0 and C represent the initial and current concentrations of the pollutant, respectively. The degradation kinetics followed a pseudo-first-order model, described by eqn (4):[46–49]

$$\frac{C}{C_0} = e^{-kt} \tag{4}$$

where k is the first-order rate constant of the reaction (min^{-1}) at reaction time (t).

2.6.2 Polymer-based membranes' antibacterial activity

2.6.2.1 Pre-inoculum preparation. The antimicrobial activity of the membranes was tested using Gram-positive *Staphylococcus epidermidis* (NCTC 11,047) and Gram-negative *Escherichia coli* k12 (NCTC 10538) strains obtained from The National Collection of Type Cultures (NCTC). The pre-inocula were prepared by suspending a single colony from stock cultures in nutrient broth (NB) and incubating overnight at 37 °C with shaking at 110 rpm.

2.6.2.2 Antibacterial activity. The bactericidal activity of the membranes was evaluated using a modified version of the ASTM-E2149-01 standard shake flask method. Bacterial cells from the pre-inoculum were harvested through two rounds of centrifugation (5000 rpm for 5 min) and resuspended in a 0.9% NaCl (w/v) solution. The suspension's optical density (OD) was measured at 600 nm and adjusted to 0.1, corresponding to an inoculum of approximately 1×10^6 CFU mL^{-1}. Simultaneously, membrane pieces (1×1 cm^2) were sterilised under UV light before testing. The inoculum was combined with the samples and incubated at 37 °C with shaking at 200 rpm for 2 hours. The resulting suspensions were serially diluted in sterile 0.9% NaCl (w/v), plated onto NB agar, and incubated at 37 °C for 24 hours to quantify surviving bacterial colonies. The reduction in bacterial counts was expressed as $\log_{10}$ reduction, providing quantitative data on the membrane's antibacterial efficacy compared to control conditions (no material).

2.6.2.3 Polymer-based membranes induced ROS formation. A lamp that mimics the sunlight (FL T8–900 mm 30 W Sylvania), which had previously been placed in the incubator, was used to apply the light stimuli to the samples and further quantification of the reactive oxygen species (ROS). The samples were in contact with the bacterial inoculum for 2 h at 37 °C and 200 rpm in the incubator with the sun-mimicking light (SLM). The samples incubated without stimuli were used as controls. Then, the probe 2-7-dichlorodihydrofluorescein diacetate ($DCFH_2$-DA) at a final concentration of 10 μM was added to the bacterial solution and incubated at 37 °C for 20 min. The $DCFH_2$-DA was used as a substrate for quantitatively measuring the intracellular oxidant production. This non-fluorescent molecule is oxidised to the fluorescent 2-7-dichlorofluorescein (DCF) by the action of bacterial cellular oxidants. The DCFH fluorescence intensity was detected using a multimode reader at an excitation wavelength of 488 nm and an emission wavelength of 525 nm to further quantify the ROS level.

3 Results and discussion

3.1 Synthesis and characterisation of nanoparticles

The inorganic-organic hybrid (TiO_2/5-ASA/Ag) was synthesised to improve performance in eliminating bacteria and degradation of antibiotics by photo-driven reactions. The initial synthesis step in forming the ICT complex between TiO_2 and 5-ASA. This was achieved through a condensation reaction involving the surface hydroxyl groups of both inorganic and organic components.[80,81] The amino group from 5-ASA remains free, thus enabling its role in the subsequent step, whereby it reduces Ag^+ ions and facilitates the attachment of the formed Ag NPs to the TiO_2/5-ASA. The TEM analysis of the TiO_2/5-ASA/Ag nanocomposites (Fig. 2a and b) reveals the presence of small (<5 nm) spherical Ag NPs distributed randomly across the surface of the commercial TiO_2 nanoparticles. The XRD pattern

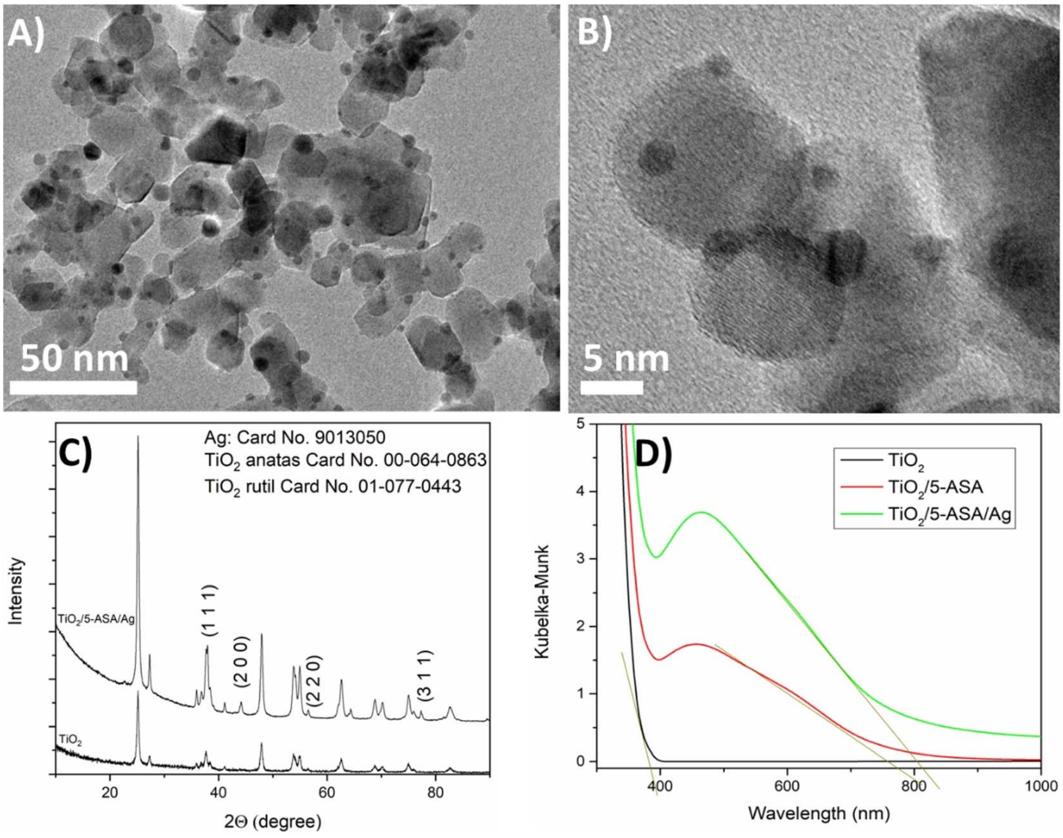

Fig. 2 (a) Low- and (b) high-magnification TEM images of TiO_2/5-ASA/Ag nanocomposites. (c) XRD of TiO_2/5-ASA/Ag nanocomposites. (d) Kubelka–Munk transformation of reflection spectra of commercial TiO_2 and synthesised TiO_2/5-ASA and TiO_2/5-ASA/Ag nanocomposites.

of the TiO_2/5-ASA/Ag nanocomposite is presented in (Fig. 2c). The indexed diffraction peaks at 37.9, 44.2, 64.2, and 77.3° correspond to the (111), (200), (220), and (311) crystal planes of face-centred-cubic silver, respectively (card no. 9013050). The remaining diffraction peaks at 25.3° and 48.0° (anatase) and 27.3° and 54.1° (rutile) originate from commercial Degussa P25 (000640863 and 000211276 are card numbers of anatase and rutile phases, respectively). XRD did not detect the small amount of 5-ASA and Ag on the surface of TiO_2 due to low amounts and reduced nanoparticle size. Additionally, there are no changes in the diffractogram of TiO_2/5-ASA/Ag when compared to the pristine TiO_2, indicating that the functionalisation of TiO_2 with ASA and Ag did not modify the crystalline structure of the nanocatalysts.

The composition of the TiO_2/5-ASA/Ag composite was estimated using the ICP-OES technique after digesting the hybrid with concentrated HNO_3 and H_2O_2. The experimental data indicated 58 and 2.6 wt% of Ti and Ag in the TiO_2/5-ASA/Ag composite, respectively. Assuming a stoichiometric ratio between Ti and O in TiO_2, the content of TiO_2 is around 96.5 wt%, while the remaining, about 1 wt%, is the content of the organic phase (5-ASA), as data available in Table S1 in SI.

Optical changes after each synthetic step were followed by diffuse reflection spectroscopy. The Kubelka–Munk transformations[87] of diffuse reflection data for TiO_2, TiO_2/5-ASA, and TiO_2/5-ASA/Ag nanoparticles are shown in (Fig. 2d).

Unmodified TiO_2 has a steep absorption increase towards the UV spectral range starting from 400 nm. The TiO_2/5-ASA displays a significant redshift with an absorption onset close to 800 nm induced by the ICT complex formation. The calculated band gap, determined from the reflectance spectra, is 3.8 and 1.6 eV for TiO_2 and TiO_2/5-ASA, respectively. The presence of free electron-donating functional groups in the organic component of the ICT complex, in this case, amino groups, additionally shifts absorption towards the near-infrared spectral region compared to the ICT complex with an organic component without these types of functional groups.[88] The optical properties of the TiO_2/5-ASA/Ag hybrids are similar to the TiO_2-based ICT complex with 5-ASA, since there is an overlap between the absorption of TiO_2/5-ASA and the expected position of the surface plasmon resonance band of a nanometre in size Ag NPs.[89]

3.2 Polymer-based membranes characterisation

After characterising the synthesised nanoparticles and confirming their structural and optical properties, they were added to porous polymeric matrices to obtain a nanocomposite membrane with photocatalytic and antimicrobial properties. The polymeric matrix exploited for the nanocomposite development was PVDF-HFP, a synthetic and highly stable polymer, and SF, a naturally derived polymer. SEM images of the membranes (Fig. 3A) indicate the formation of well-distributed micrometric porous structures by TIPS due to the thermally induced phase separation process and the slow evaporation of the solvent,[90] the addition of NaCl as a porogen promotes the formation of highly porous materials, regardless of the polymer used.[41] Adding TiO_2/5-ASA and TiO_2/5-ASA/Ag nanoparticles to the PVDF-HFP polymer matrix did not result in a significant alteration of the membrane microstructure, nor did it promote the formation of agglomerates compared to the pristine membrane (Fig. 3A). Similarly, the morphology of the SF matrix remained unchanged between the pure membrane and the addition of NPs, maintaining a highly porous microstructure with interconnected pores (Fig. 3B).

Contact angle measurements were performed to assess the membranes' wettability. The PVDF-HFP-based membranes revealed the typical hydrophobic behaviour, with the contact angle increasing from 95° for the pristine PVDF-HFP membrane to 130° when the nanoparticles are incorporated into the

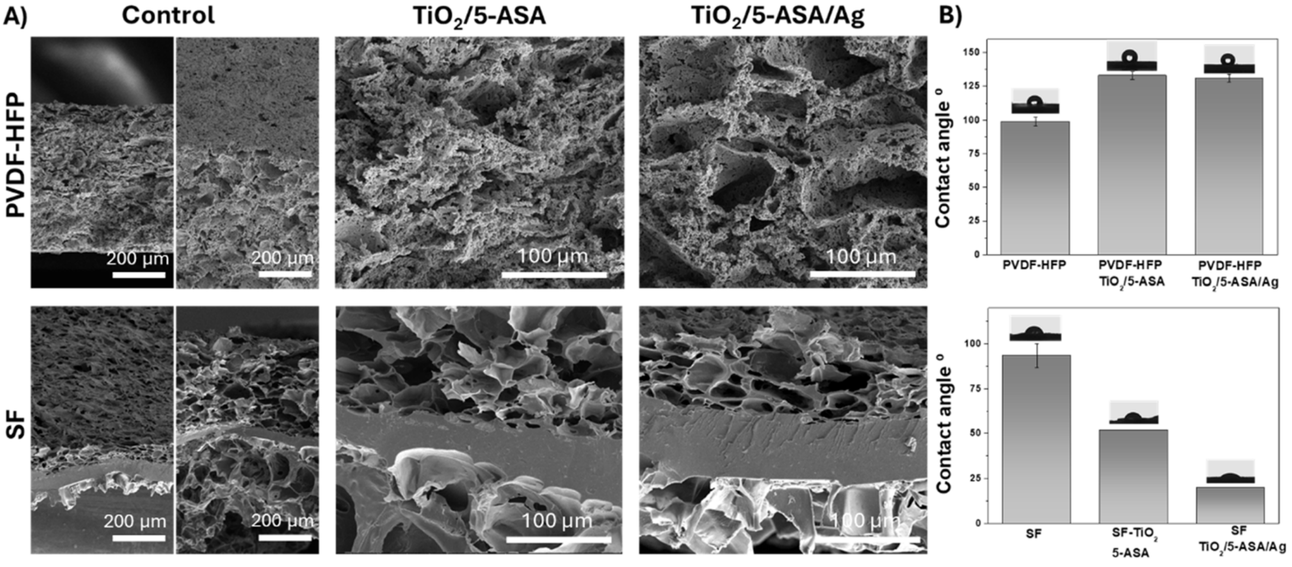

Fig. 3 (A) Cross-sectional and tilted SEM images of porous membranes composed of PVDF-HFP and SF with TiO_2/5-ASA and TiO_2/5-ASA/Ag fillers. SEM images of controls are at 250× magnification, while fillers are at 1000× magnification. (B) Contact angle of the different membranes.

polymeric matrix (Fig. 3B). These findings align with the results reported in the literature.[7,83]

Conversely, in SF-based membranes, the samples are hydrophilic, and incorporating NPs enhances their hydrophilicity. The contact angle highly decreases from 90° for SF membranes to 50° in the case of SF : TiO_2/5-ASA and to 20° in the case of SF : TiO_2/5-ASA/Ag (Fig. 3B), a fact that increased hydrophilicity with the incorporation of fillers, which has been previously reported.[91]

FTIR and DSC techniques, respectively, were used to investigate the chemical and thermal properties of the produced membranes (Fig. 4).

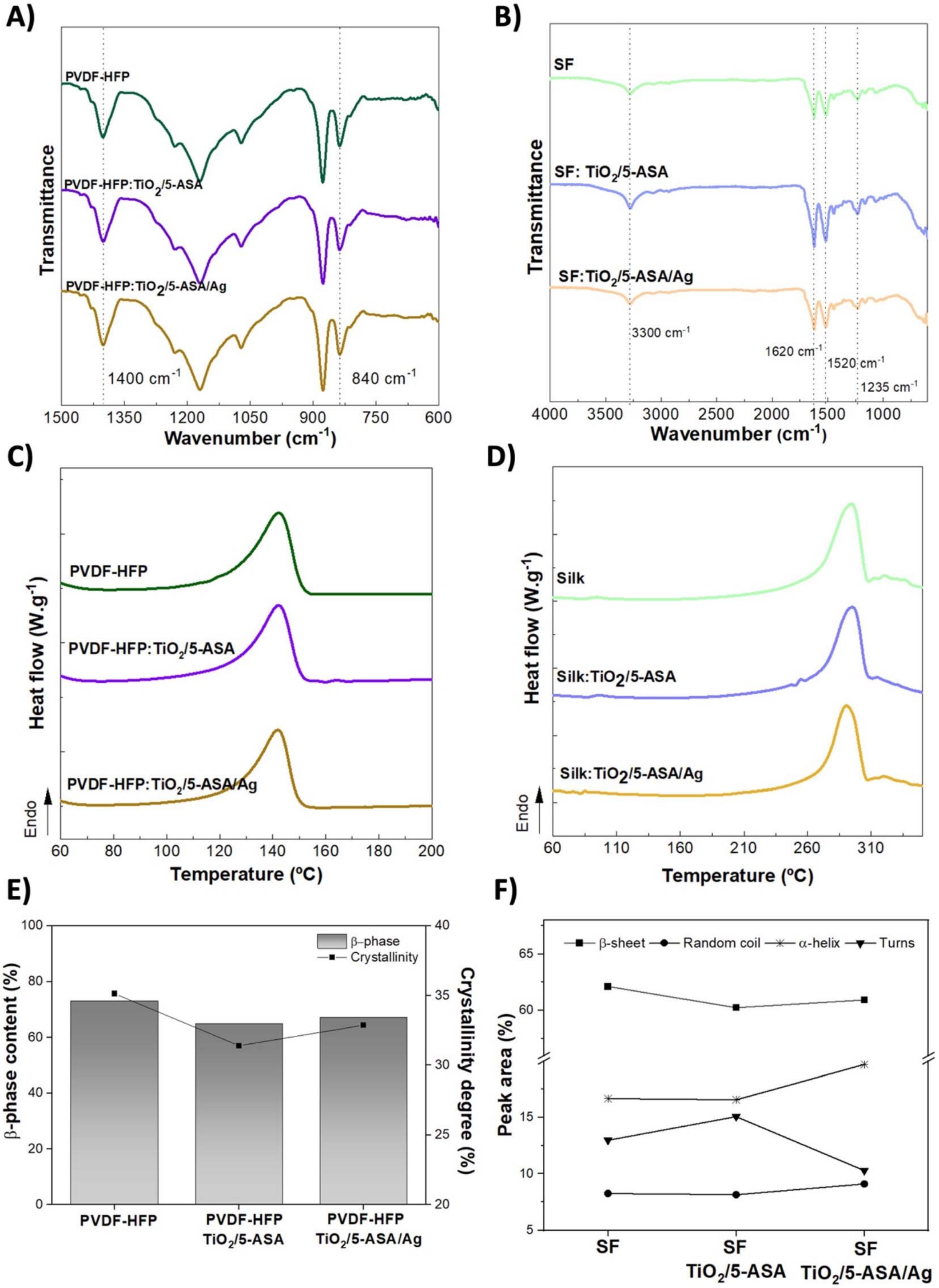

Fig. 4 FTIR spectra of the (A) PVDF-HFP-based and (B) SF-based membranes; DSC thermograms of the (C) PVDF-HFP-based and (D) SF-based membranes; (E) β-phase quantification and degree of crystallinity of PVDF-HFP-based membranes and (F) secondary structures of SF-based membranes disclosed by deconvolution of the amide I bands.

FTIR analysis assessed the vibrational bands of the polymer matrices before and after the incorporation of nanoparticles, thereby providing insight into potential chemical interactions between the polymer and nanoparticles. The FTIR spectra of the PVDF-HFP-based membranes (Fig. 4A) reveal the presence of characteristic bands associated with the β-phase of the polymer, specifically at 840 and 1400 cm^{-1}, and the α-phase at 766 cm^{-1}.[42,92]

The calculated β-phase content for each PVDF-HFP-based membrane (eqn (1)) is illustrated in Fig. 4E, demonstrating that the β-phase is the predominant phase across all membranes, irrespective of nanoparticle addition. This observation aligns with previous findings indicating that solvent evaporation at room temperature predominantly induces the crystallisation of PVDF-HFP in the electroactive β-phase.[41,44,48,85] However, a slight reduction in β-phase content is observed upon nanoparticle incorporation, which can be attributed to electrostatic interactions between the polymer and nanofillers during crystallisation, consistent with existing literature.[7]

Fig. 4B presents the FTIR spectra of SF-based membranes. The primary absorption bands for SF are observed at approximately 3300 cm^{-1} (NH stretching), 1620 cm^{-1} (C═O stretching), 1520 cm^{-1} (CN stretching and NH bending), and 1235 cm^{-1} (C–N stretching), which correspond to Amide A, Amide I, Amide II, and Amide III, respectively.[93] All these absorption bands can be observed in the spectra, indicating that the primary structure of the SF-based membranes is preserved even when nanoparticles are incorporated. The secondary structure of SF-based membranes was also investigated by analysing the Amide I region at 1700–1580 cm^{-1}. The Amide I band deconvolution allowed to determine the relative amount of β-sheet, random coils, α-helix and turns conformations in each sample (Fig. 4F). The β-sheet conformation is the most prevalent, accounting for more than 60% of the total amide I peak area in all samples. Thus, according to the degree of crystallinity formula for SF compounds,[94] the SF-based membranes exceed 60% crystallinity, with the pristine SF membrane exhibiting the highest values. On the other hand, in nanoparticle-containing samples, the random coil structure and α-helix increase compared to pristine ones, which suggests a slight preference for amorphous conformation. This implies that nanoparticles act as a steric impediment, restricting protein chains from totally packing and thus crystalline units from stabilising.

DSC measurements were also performed, which allowed to study the melting temperature and the degree of crystallinity of the membranes. Observing the DSC thermograms from PVDF-HFP-based membranes (Fig. 4C), all the samples showed similar behaviour with a single endothermic peak around 141 °C corresponding to the melting temperature of the polymers.[41,86] Incorporating the nanoparticles did not significantly change the thermal stability of the crystalline phase, with a melting temperature for the composites similar to that of the pristine PVDF-HFP.

The calculated degree of crystallinity of the PVDF-HFP-based membranes is shown in Fig. 4E. All the samples presented a degree of crystallinity higher than 30%.[48] However, the incorporation of nanoparticles led to a decrease in the crystallinity of the membranes,[41] as the nanoparticles acted as the defect during the crystallisation process of the polymer.[95] The DSC thermograms of SF-based membranes (Fig. 4D) show that all membranes exhibit similar behaviour regardless of the addition of nanoparticles, indicating an endothermic peak around 290 °C,[96] attributed to the thermal degradation of protein chains, essentially the decomposition of β-sheet crystalline units.[97]

3.3 Photocatalytic performance of nanocomposite membranes

The ability of the membranes to degrade CIP through the photocatalytic process was evaluated under UV and VIS irradiation over time, with samples being withdrawn at determined time intervals for UV-vis spectroscopy analysis and monitoring of the highest absorbance peak of CIP (277 nm) (Fig. 5 and summarised in Table 1).[9] Before performing the photocatalytic tests with the produced samples, the photostability of CIP was evaluated under UV irradiation for 600 minutes, demonstrating residual or slight degradation (0.006%) – Fig. S2A. Afterwards, the photocatalytic activity of the pure PVDF-HFP membranes and the PVDF-HFP/TiO_2 and PVDF-HFP/Ag/TiO_2 nanocomposites under UV irradiation was evaluated. It is essential to note that all samples were left in the dark for 30 minutes to reach the CIP adsorption/desorption equilibrium with the produced pure polymeric and nanocomposite membranes. The pure PVDF-HFP sample and the PVDF/TiO_2/5-ASA/Ag sample did not reveal any adsorption, and only the PVDF-HFP/TiO_2/5-ASA sample showed a slight adsorption of approximately 5%. These results confirm the low affinity of CIP towards the matrix and the photocatalytic nanoparticles in the absence of radiation. Then, UV irradiation was started, and there was no CIP degradation for the pure PVDF-HFP membrane. The PVDF-HFP/TiO_2/5-ASA and PVDF/TiO_2/5-ASA/Ag nanocomposite samples showed ≈38% and ≈63% of CIP photocatalytic degradation after 600 minutes of irradiation, respectively.

Similarly, the SF/TiO_2/5-ASA and SF/TiO_2/5-ASA/Ag membranes exhibit ≈38% and ≈50% photocatalytic activity efficiencies for the same experimental conditions. These results, obtained with PVDF-HFP and SF-based membranes, along with the calculated reaction rates summarised in Table S2 in the SI, demonstrate the significant improvement in the pollutant's photocatalytic degradation efficiency when Ag is added to the nano photocatalyst, which is approximately 1.7 in PVDF-HFP membranes and 1.3 in the case of the SF.

Functionalizing TiO_2/5-ASA with Ag improved the degradation efficiency of CIP under UV irradiation regardless of the polymeric matrix. Literature has already addressed this phenomenon, indicating that Ag nanoparticles in the mesoporous TiO_2 structure can induce a Schottky junction at the interface, thus introducing intermediate energy levels.[98] When excited, electrons from the conduction bands (CB) transfer to the Ag nanoparticles while the holes in the valence band (VB) are retained in the TiO_2, decreasing electron–hole recombination and prolonging the lifetime of the holes generated. As

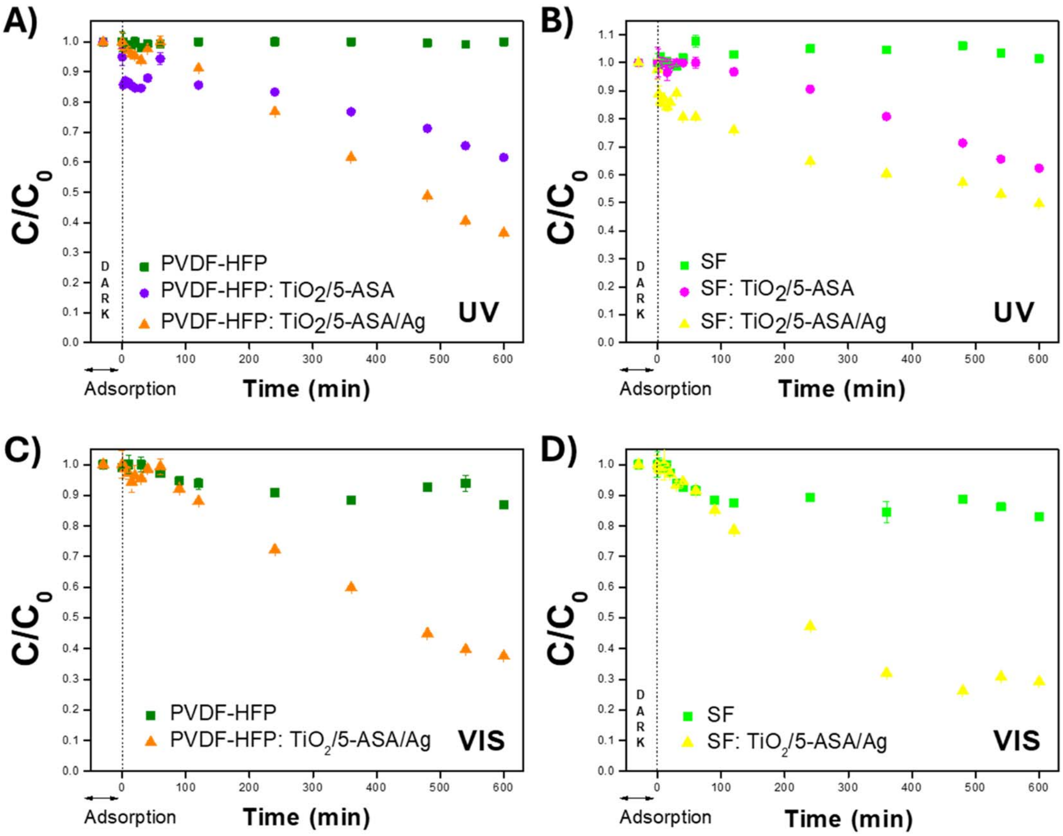

Fig. 5 Photocatalytic degradation of CIP ($C_0 = 5$ mg L^{-1}) with (A) PVDF-HFP and (B) SF-based membranes over 600 min of UV irradiation; with (C) PVDF-HFP and (D) SF-based membranes over 600 min of VIS irradiation.

Table 1 CIP degradation efficiencies (%) under UV and VIS radiation for the different pristine and nanocomposite membranes

	Degradation (%)	
Sample	UV	Simulated sunlight (VIS)
PVDF-HFP	≅ 0	13.1
PVDF-HFP : TiO$_2$/5-ASA	38.4	—
PVDF-HFP : TiO$_2$/5-ASA/Ag	63.4	62.4
SF	≅ 0	16.9
SF : TiO$_2$/5-ASA	37.6	—
SF : TiO$_2$/5-ASA/Ag	50.3	70.8

a result, the photocatalytic activity of the composite is enhanced.[40,99] Additionally, it has been shown that Ag in the nanocomposite extends the TiO$_2$ absorption range from UV to visible regions through surface plasmon resonance, coupled with a band gap reduction.[100] These findings are backed up by the characterisation of the nanoparticles, which reveals reflectance in the visible range (~500 nm), and the calculation of the bandgap (Fig. 2D).

TiO$_2$/5-ASA/Ag nanoparticles were tested in suspension in a CIP solution under Xenon lamp irradiation to confirm this. These tests revealed degradation efficiencies of ~84% in 90 minutes of exposure (Fig. S1A and S1B), which corroborates the findings presented in previous literature.[11,101] After confirming the ability of the particles to absorb visible radiation, we have also assessed the photocatalytic activity of the TiO$_2$/5-ASA/Ag nanoparticles immobilised into PVDF-HFP and SF matrices under a Xenon lamp irradiation for 600 min (Fig. 5C and D). Similarly to the UV assays, the first tests were performed with the pristine membranes under simulated sunlight irradiation (VIS), revealing a CIP removal of 13% for PVDF-HFP and about 17% for SF.

Regarding the nanocomposite membranes, the PVDF-HFP : TiO$_2$/5-ASA/Ag membrane degradation efficiency overperformed by attaining 62% of ciprofloxacin degradation. SF : TiO$_2$/5-ASA/Ag membrane degradation efficiency accomplished values higher than 71%, representing an increase of 49% and 54% compared to the corresponding controls, PVDF-HFP and SF (Table 1). Considering that the photocatalytic nanoparticles used in both polymeric nanocomposite membranes are the same and that the porous microstructure resembles both polymer matrices, it is possible to understand that the obtained microstructure is superimposed over wettability. In detail, the photocatalytic results obtained with the PVDF-HFP-based matrices (hydrophobic Fig. 3B) are similar to the ones obtained with the SF-based membranes (hydrophilic Fig. 3B). Thus, the employed processing method, salt leaching combined with solvent casting, led to interconnected pores in both polymer matrices, which is essential for the percolation of the solution across the porous microstructure of the membrane, more easily exposing the photocatalytic nanoparticles to contact with CIP, leading to increasing degradation efficiency. This processing method allowed the creation of similar porous microstructures for the PVDF-HFP and SF matrices, which also aids in explaining the similarities of the obtained results. To wrap up, the use of natural polymer matrices is validated in comparison with a synthetic polymer, which results from the proper processing of the polymer and porous tuning.

The literature extensively reports the incorporation of fillers on polymeric substrates for photocatalytic applications.[102,103] Semiconductors such as TiO_2 have been mentioned to be incorporated into substrates such as polyethylene terephthalate (PET) for degrading antibiotics like trimethoprim. The composite has exhibited a degradation efficiency of 90%, utilising a UV radiation intensity of 500 W m^{-2} and an initial concentration five times lower than that employed in this study.[104] Previous studies have also reported NPs functionalised with noble metals, such as Au/TiO_2. For instance, 10% of these particles were immobilised on PVDF-HFP membranes to degrade norfloxacin, an antibiotic from the same group as the one used in this paper, yielding similar degradation rates of 2×10^{-3} min^{-1}.[39] Natural polymers have also been used as substrates for immobilising photocatalysts. *Yontar et al.*[105] processed polyvinyl alcohol (PVA) films by TIPS with 25% photocatalytic plant extracts, with the result that 0.2 g of film was capable of removing 61.3% of methylene blue (10 mg L^{-1}). Chitosan was used as a matrix for copper (Cu) in degrading Congo red dye, demonstrating high removal efficiencies for three consecutive cycles.[106]

The study presents an innovative approach to the green functionalisation of nanoparticles within a natural polymer. This exploits the synergy with SF's porous microstructure, providing a sustainable and efficient alternative to the typical photocatalytic materials. This sustainable method efficiently degrades emerging contaminants and explores solar radiation as a renewable energy source, with no similar research published to date.

3.3 Reusability of the SF : TiO_2/5-ASA/Ag membranes

Since the reuse of PVDF has already been studied[11,38] and on the other hand, SF represents a more sustainable approach, where its reuse is less studied; therefore, a study on the reuse of SF : TiO_2/5-ASA/Ag membranes for three cycles under UV and simulated solar irradiation was performed. The results are presented in Fig. 6A and C (UV irradiation) and Fig. 6B and D (simulated solar irradiation). The experiments were carried out to assess the reproducibility of the material and its reusability. The same experimental conditions were employed as those previously described, in which the membranes were washed with ultrapure water and dried at room temperature between uses before returning to contact with a fresh CIP solution and radiation exposure.

The analysis of the results regarding the degradation efficiencies of the first and the third use shows that the particles and the polymer are efficiently attached, corroborated by the low efficiency losses, which are around 9% and 6% for UV and

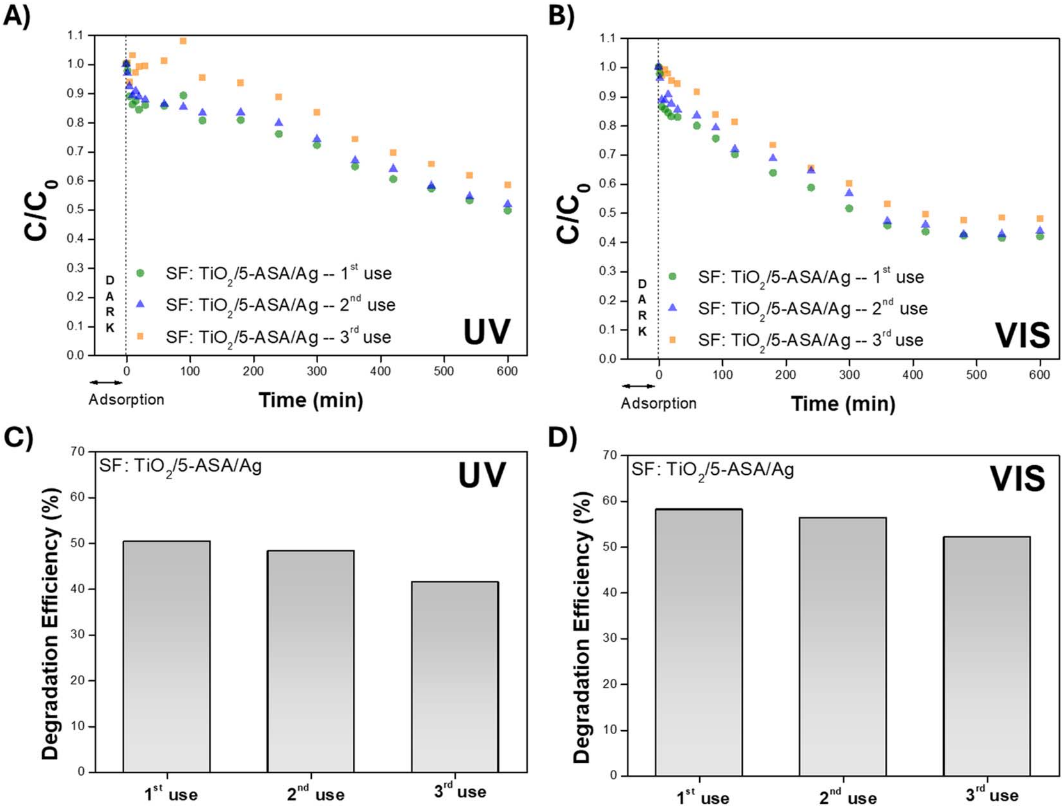

Fig. 6 Photocatalytic degradation of CIP ($C_0 = 5$ mg L^{-1}) in three consecutive uses of SF : TiO_2/5-ASA/Ag membranes irradiated for 600 min with (A) UV, (B) VIS and their respective degradation efficiency (%) in (C) and (D).

VIS degradation (Fig. 6C and D).[107] This agrees with what is reported in the literature, where, for instance, Momeni *et al.*, observed losses of 7% after cycles of methylene blue degradation.[108] Furthermore, in another study, Zhou *et al.* used Ag@AgCl on polyurethane/silk fibroin porous films to degrade a model organic pollutant (Rhodamine B). The composite material was subjected to consecutive cycles, resulting in slightly more significant efficiency losses than those obtained in this work.[109] An inefficient immobilisation or a more superficial deposition of the particles is pointed out as one of the possible causes of the leaching of the particles for the loss of efficiency in CIP degradation after the first use.[110]

The herein produced SF-based membrane has demonstrated suitability for immobilising photocatalysts, as evidenced by the high efficiencies and low reuse losses observed, indicating the stability of the produced membranes. If the microstructure of the membrane or the attachment of nanoparticles were compromised, the efficiency loss would have increased significantly between uses. Ultimately, this approach constitutes a green and biodegradable alternative to synthetic membranes in terms of performance and long-term stability.

3.4 Antimicrobial properties of nanocomposite membranes

The antimicrobial performance of the membranes was also evaluated towards *S. epidermidis* and *E. coli*, herein used as Gram-positive and Gram-negative bacteria models. While *E. coli* and *S. epidermidis* are bacteria commonly found in various environments, including on surfaces and in materials, *E. coli* is commonly found in contaminated water, posing significant risks to human health and the environment.[111]

Overall, *E. coli* was found to be more susceptible to both silk and PVDF-based materials, showing higher bacterial $\log_{10}$ reductions when compared to *S. epidermidis* (Fig. 7A and B). When the nanoparticles were present in the material, bacterial load was reduced for *E. coli* 1–2 $\log_{10}$ and *S. epidermidis* 0.5 $\log_{10}$, mainly when the particles were functionalised with silver (Fig. 7A and B). Silver has long been recognised as a potent antimicrobial due to its ability to disrupt cell membranes, bind to proteins, interfere with DNA, and generate ROS oxygen species, which collectively inhibit bacterial growth.[112] Nevertheless, since the material was found to possess photocatalytic properties, mainly in the presence of silver, due to the shift in the plasmon resonance of the particles to the visible range, making them able to induce the formation of ROS through photocatalytic events (Fig. S1a and b), a quantification of ROS was performed.

Thus, besides the antimicrobial effect of silver, it is acceptable to assume that the formation of ROS can disrupt the bacterial cell's structure and function, ultimately killing the microorganisms. Thus, to prove this concept, the quantification of ROS on the most susceptible bacterium (*E. coli*), after applying a sun-mimicking light (VIS), was performed (Fig. 7C

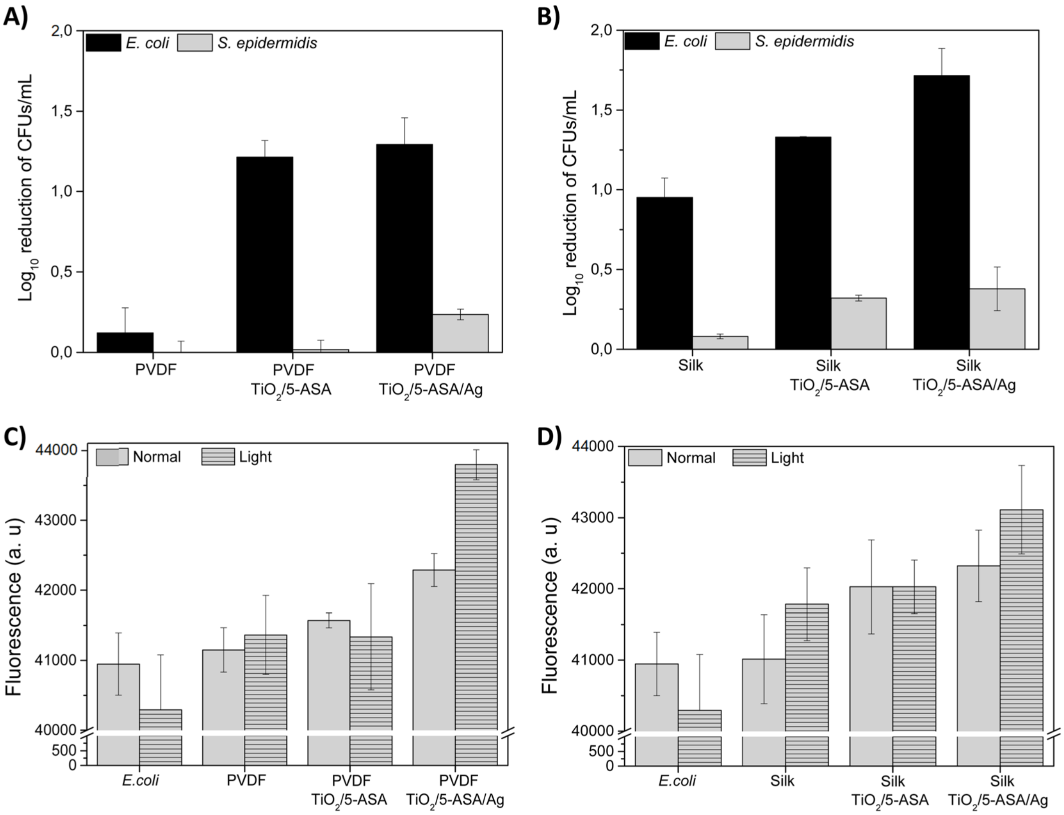

Fig. 7 . Antibacterial activity of (A) PVDF-HFP-based membranes and (B) SF-based membranes in terms of *E. coli* and *S. epidermidis* $\log_{10}$ reduction, and dichlorofluorescein fluorescence intensity in *E. coli* in contact with (C) PVDF-HFP-based membranes and (D) SF-based membranes, in "normal" conditions and after application of the sun-mimicking light.

and D). According to the results, this light, which includes UV wavelengths typically present in the sunlight (3–5%), induces the highest percentage of ROS. This finding demonstrates that developing photocatalytic materials engineered to produce ROS makes them valuable for antibacterial purposes. Nevertheless, it is essential to highlight that ROS formation is present even in typical bacterial cultures without light.[113] Some nanoparticles, particularly those made of TiO_2 and Ag, can undergo chemical reactions or even release ions, resulting in the generation of ROS.

As mentioned before, the effect of the tested material, regardless of the type of matrix used, was more pronounced with *E. coli*, which is one of the most problematic bacteria in the environment.[114] The differences in the cell wall's composition and the outer membrane of the bacteria used herein may be the reason why *E. coli* is more susceptible compared to *S. epidermidis*. *E. coli* is a Gram-negative bacterium with a thinner peptidoglycan layer in its cell wall compared to *S. epidermidis*, a Gram-positive bacterium with a thicker peptidoglycan layer. The thinner cell wall of *E. coli* may make it more susceptible to damage from physical and chemical agents present in materials.[115] Moreover, *E. coli* has an outer membrane that contains lipopolysaccharides (LPS), which can be more susceptible to disruption by certain materials or environmental conditions.[116] This outer membrane provides less protection than the thick peptidoglycan layer of Gram-positive bacteria like *S. epidermidis*.

4. Conclusions

Aquatic contamination constitutes a global crisis for the present and future of the environment and humanity. New technologies and materials that can efficiently remove persistent contaminants, such as ciprofloxacin (CIP), are needed. This study successfully employed a green approach to produce TiO_2 nanoparticles functionalised with salicylic acid and smaller Ag nanoparticles (TiO_2/5-ASA and TiO_2/5-ASA/Ag), endowing the pristine TiO_2 material with the absorption of visible range radiation. This was experimentally confirmed by band gap reduction from 3.6 to 1.6 eV and photocatalytic degradation of CIP under simulated solar radiation (% deg) using TiO_2/5-ASA and TiO_2/5-ASA/Ag nanoparticles. Afterwards, these active nanoparticles were immobilised into two different polymer matrices: high-performing synthetic PVDF-HFP and natural Silk Fibroin – SF. The same solvent casting and salt leaching techniques were employed to obtain an interconnected, highly porous microstructure in both PVDF-HFP and SF membranes. The characterisation of the nanocomposite membranes indicated that incorporating the TiO_2/5-ASA and TiO_2/5-ASA/Ag nanoparticles into the polymer matrices did not significantly change the membrane's physical–chemical properties, confirming the robustness of both polymeric photocatalytic nanocomposites. The PVDF-HFP : TiO_2/5-ASA/Ag sample outperformed, degrading 63 and 62% of CIP under UV and simulated solar irradiation, respectively. The SF : TiO_2/5-ASA/Ag nanocomposites accomplished 50 and 71% degradation under the same conditions and retained their efficiency with a loss of less than 10% loss after three consecutive cycles. These results validate solvent casting and salt leaching techniques for synthetic and natural polymer matrices for photocatalytic applications. Furthermore, the distinct physicochemical characteristics of the membranes illustrate a variation in nanoparticle encapsulation, which may lead to disparate performances between PVDF-HFP and SF. When considered alongside their natural origins, SF membranes could be utilised in diverse aquatic environments with varying contaminants, potentially supplanting high-performance polymers. The validation of SF nanocomposite membranes' reusability is also paramount, as natural-based materials are commonly associated with low reusability/robustness. The materials evaluation also confirmed the antimicrobial properties of all the nanocomposites containing Ag, with a reduction in bacterial load by 1–2 $\log_{10}$, likely due to ROS formation.

In short, this work lays a solid foundation for the future of multifunctional materials based on natural polymers in water decontamination. Employing the robust processing technique can mitigate intrinsic material differences, favouring their efficient functional practicability.

Data availability

The data supporting this article have been included as part of the SI.

The SI includes details on the synthesis and functionalization of TiO_2 nanoparticles with 5-aminosalicylic acid and silver, their incorporation into PVDF-HFP and silk fibroin membranes, and the characterisation techniques employed (ICP-OES, UV-vis spectroscopy, and antimicrobial assays). It also describes the experimental procedures for photocatalytic degradation of ciprofloxacin under UV and visible light, antimicrobial tests against Gram-positive and Gram-negative bacteria, photolysis studies, and kinetic analyses of degradation rates. See DOI: **https://doi.org/10.1039/d5su00569h**.

Conflicts of interest

There are no conflicts of interest to declare.

Acknowledgements

The authors thank the Fundação para a Ciência e Tecnologia (FCT) for financial Support under the framework of Strategic Funding UID/04050 – Centro de Biologia Molecular e Ambiental and UID/FIS/04650/2020. The HORIZON-MSCA-2022-SE-01-01 SELFAQUASENS (101131379) project, which received funding from the European Union's Horizon Europe Research and Innovation Programme, is also acknowledged. JMQ thanks the FCT for the fellowship 10.54499/2021.08822.BD; FZ acknowledges support from the European Union's Horizon Europe Research and Innovation Programme under the Marie Skłodowska-Curie HORIZON-MSCA-2023-PF-01-01 3DMemBio (101151986), and from Basque Government under the postdoctoral fellowship (POS_2023_1_0033). PMM for contract **https://doi.org/10.54499/2020.02802.CEECIND/CP1600/CT0017** and MMF for contract CEECINST/00018/2021/CP2806/CT0010. RBP thanks the Ministry of Economy and Competitiveness for the Juan de la Cierva (JDC2023-052829-I) research contract. This study forms part of the Advanced Materials program and was supported by MCIN with funding from European Union NextGenerationEU (PRTR-C17.I1) as well as by IKUR Strategy under the collaboration agreement between Ikerbasque Foundation and Fundación BCMaterials on behalf of the Department of Education of the Basque Government. Funding is from the Basque Government Industry Department under the ELKARTEK program, which is also acknowledged. The Serbian team was supported by the Ministry of Science, Technological Development and Innovation of the Republic of Serbia (contract number 451-03-136/2025-03/200017) and by the Science Fund of the Republic of Serbia, Program PRISMA, grant no. 5354, Multifunctional visible-light-responsive inorganic-organic hybrids for efficient hydrogen production and disinfection-HYDIS.

References

1 R. P. Schwarzenbach, T. Egli, T. B. Hofstetter, U. Von Gunten and B. Wehrli, *Annu. Rev. Environ. Resour.*, 2010, **35**, 109–136.
2 G. I. Tovar, A. Valverde, C. Mendes-Felipe, S. Wuttke, A. Fidalgo-Marijuan, E. S. Larrea, L. Lezama, F. Zheng, J. Reguera, S. Lanceros-Méndez, M. I. Arriortua, G. Copello and R. F. de Luis, *ChemSusChem*, 2021, **14**, 2892–2901.
3 W. H. Organization, *Progress on Household Drinking Water, Sanitation and Hygiene 2000-2017: Special Focus on Inequalities*, World Health Organization, 2019.
4 U. N. E. Programme, *Making Peace with Nature - A Scientific Blueprint to Tackle the Climate, Biodiversity and Pollution Emergencies*, Nairobi, 2021.
5 T. B. Cetrulo, R. C. Marques, T. F. Malheiros and N. M. Cetrulo, *Sci. Total Environ.*, 2020, **727**, 138746.
6 A. K. Yadav, H. K. Yadav, A. Naz, M. Koul, A. Chowdhury and S. Shekhar, *Environ. Adv.*, 2022, **9**, 100262.
7 L. Aoudjit, H. Salazar, D. Zioui, A. Sebti, P. M. Martins and S. Lanceros-Mendez, *Polymers*, 2021, **13**, 3718.
8 S. Dey, F. Bano and A. Malik, in *Pharmaceuticals and Personal Care Products: Waste Management and Treatment Technology*, Elsevier, 2019, pp. 1–26.
9 F. Zheng, J. M. Queirós, P. M. Martins, R. F. de Luis, A. Fidalgo-Marijuan, J. L. Vilas-Vilela, S. Lanceros-Méndez and J. Reguera, *Colloids Surf., A*, 2023, **671**, 131594.
10 A. R. Bracamontes-Ruelas, L. A. Ordaz-Díaz, A. M. Bailón-Salas, J. C. Ríos-Saucedo, Y. Reyes-Vidal and L. Reynoso-Cuevas, *Processes*, 2022, **10**, 1041.
11 H. Salazar, P. Martins, B. Santos, M. Fernandes, A. Reizabal, V. Sebastián, G. Botelho, C. J. Tavares, J. L. Vilas-Vilela and S. Lanceros-Mendez, *Chemosphere*, 2020, **250**, 126299.
12 D. Yadav, S. Rangabhashiyam, P. Verma, P. Singh, P. Devi, P. Kumar, C. M. Hussain, G. K. Gaurav and K. S. Kumar, *Chemosphere*, 2021, **272**, 129492.
13 I. C. Vasilachi, D. M. Asiminicesei, D. I. Fertu and M. Gavrilescu, *Water*, 2021, **13**, 181.
14 N. J. D. Reyes, F. K. F. Geronimo, K. A. V. Yano, H. B. Guerra and L.-H. Kim, *Water*, 2021, **13**, 1159.
15 U. Szymańska, M. Wiergowski, I. Sołtyszewski, J. Kuzemko, G. Wiergowska and M. K. Woźniak, *Microchem. J.*, 2019, **147**, 729–740.
16 J. Lach, L. Stępniak and A. Ociepa-Kubicka, *Probl. Ekorozwoju*, 2018, 13.
17 L. S. Redgrave, S. B. Sutton, M. A. Webber and L. J. V. Piddock, *Trends Microbiol.*, 2014, **22**, 438–445.
18 T. P. Van Boeckel, C. Brower, M. Gilbert, B. T. Grenfell, S. A. Levin, T. P. Robinson, A. Teillant and R. Laxminarayan, *Proc. Natl. Acad. Sci. U. S. A.*, 2015, **112**, 5649–5654.
19 V. Homem and L. Santos, *J. Environ. Manage.*, 2011, **92**, 2304–2347.
20 P. Grenni, V. Ancona and A. B. Caracciolo, *Microchem. J.*, 2018, **136**, 25–39.
21 J. C. Nwabuife, C. A. Omolo and T. Govender, *J. Controlled Release*, 2022, **349**, 338–353.
22 S. D. Richardson and S. Y. Kimura, *Anal. Chem.*, 2019, **92**, 473–505.
23 M. Kumari and A. Kumar, *Chemosphere*, 2020, **240**, 124864.
24 R. Daghrir and P. Drogui, *Environ. Chem. Lett.*, 2013, **11**, 209–227.
25 M. Foroughi, M. Khiadani, S. Kakhki, V. Kholghi, K. Naderi and S. Yektay, *Sci. Total Environ.*, 2021, 151404.
26 T.-K. Kim, T. Kim, H. Park, I. Lee, A. Jo, K. Choi and K.-D. Zoh, *Chem. Eng. J.*, 2020, **394**, 124803.
27 R. Anjali and S. Shanthakumar, *J. Cleaner Prod.*, 2022, **378**, 134509.
28 E. Sanganyado and W. Gwenzi, *Sci. Total Environ.*, 2019, **669**, 785–797.
29 S. Kawecki, G. Kuleck, J. H. Dorsey, C. Leary and M. Lum, *Environ. Monit. Assess.*, 2017, **189**, 261.
30 P. Karaolia, I. Michael-Kordatou, E. Hapeshi, C. Drosou, Y. Bertakis, D. Christofilos, G. S. Armatas, L. Sygellou, T. Schwartz and N. P. Xekoukoulotakis, *Appl. Catal., B*, 2018, **224**, 810–824.
31 F. Biancullo, N. F. Moreira, A. R. Ribeiro, C. M. Manaia, J. L. Faria, O. C. Nunes, S. M. Castro-Silva and A. M. Silva, *Chem. Eng. J.*, 2019, **367**, 304–313.
32 N. Castro, J. M. Queirós, D. C. Alves, M. M. M. Fernandes, S. Lanceros-Méndez and P. M. Martins, *Nanomaterials*, 2024, **14**, 525.
33 I. A. Janković, Z. V. Šaponjić, M. I. Čomor and J. M. Nedeljkovic, *J. Phys. Chem. C*, 2009, **113**, 12645–12652.
34 T. D. Savić, Z. V. Šaponjić, M. I. Čomor, J. M. Nedeljković, M. D. Dramićanin, M. G. Nikolić, D. Veljković, S. D. Zarić and I. A. Janković, *Nanoscale*, 2013, **5**, 7601–7612.
35 Y. Sun, J. B. Mwandeje, L. M. Wangatia, F. Zabihi, J. Nedeljković and S. Yang, *Adv. Fiber Mater.*, 2020, **2**, 118–122.
36 Z. Barbieriková, D. Lončarević, J. Papan, I. D. Vukoje, M. Stoiljković, S. Phillip Ahrenkiel and J. M. Nedeljković, *Adv. Powder Technol.*, 2020, **31**, 4683–4690.

37 M. Shahriari-Khalaji, F. Zabihi, A. Bahi, D. Sredojević, J. M. Nedeljković, D. K. Macharia, M. Ciprian, S. Yang and F. Ko, *J. Mater. Chem. C*, 2023, **11**, 5796–5805.

38 J. M. Queirós, H. Salazar, A. Valverde, G. Botelho, R. Fernández de Luis, J. Teixeira, P. M. Martins and S. Lanceros-Mendez, *Chemosphere*, 2022, **307**, 135922.

39 P. M. Martins, B. Santos, H. Salazar, S. A. C. Carabineiro, G. Botelho, C. J. Tavares and S. Lanceros-Mendez, *Chemosphere*, 2022, **293**, 133548.

40 P. Martins, S. Kappert, H. Nga Le, V. Sebastian, K. Kühn, M. Alves, L. Pereira, G. Cuniberti, M. Melle-Franco and S. Lanceros-Méndez, *Catalysts*, 2020, **10**, 234.

41 F. Zheng, P. M. Martins, J. M. Queirós, C. J. Tavares, J. L. Vilas-Vilela, S. Lanceros-Méndez and J. Reguera, *Chemosphere*, 2023, **313**, 137630.

42 P. M. Martins, J. M. Ribeiro, S. Teixeira, D. Y. Petrovykh, G. Cuniberti, L. Pereira and S. Lanceros-Méndez, *Materials*, 2019, **12**, 1649.

43 S. Singh, H. Mahalingam and P. K. Singh, *Appl. Catal., A*, 2013, **462**, 178–195.

44 C. M. Costa, V. F. Cardoso, P. Martins, D. M. Correia, R. Gonçalves, P. Costa, V. Correia, C. Ribeiro, M. M. Fernandes and P. M. Martins, *Chem. Rev.*, 2023, **123**, 11392–11487.

45 H. Salazar, J. Nunes-Pereira, D. Correia, V. Cardoso, R. Gonçalves, P. Martins, S. Ferdov, M. Martins, G. Botelho and S. Lanceros-Méndez, *Mater. Chem. Phys.*, 2016, **183**, 430–438.

46 H. Salazar, P. M. Martins, A. Valverde, R. Fernández de Luis, J. L. Vilas-Vilela, S. Ferdov, G. Botelho and S. Lanceros-Mendez, *Adv. Mater. Interfaces*, 2022, **9**, 2101419.

47 P. Martins, B. Santos, H. Salazar, S. A. Carabineiro, G. Botelho, C. J. Tavares and S. Lanceros-Mendez, *Chemosphere*, 2022, **293**, 133548.

48 C. Ribeiro, C. M. Costa, D. M. Correia, J. Nunes-Pereira, J. Oliveira, P. Martins, R. Gonçalves, V. F. Cardoso and S. Lanceros-Mendez, *Nat. Protoc.*, 2018, **13**, 681–704.

49 F. Zheng, P. M. Martins, J. M. Queirós, C. J. Tavares, J. L. Vilas-Vilela, S. Lanceros-Méndez and J. Reguera, *Int. J. Mol. Sci.*, 2022, **23**, 13741.

50 P. Yadav, N. Ismail, M. Essalhi, M. Tysklind, D. Athanassiadis and N. Tavajohi, *J. Membr. Sci.*, 2021, **622**, 118987.

51 I. Jahan and L. Zhang, *J. Polym. Environ.*, 2021, 1–21.

52 R. Lohmann, I. T. Cousins, J. C. DeWitt, J. Gluge, G. Goldenman, D. Herzke, A. B. Lindstrom, M. F. Miller, C. A. Ng and S. Patton, *Environ. Sci. Technol.*, 2020, **54**, 12820–12828.

53 H. S. Auta, C. Emenike and S. Fauziah, *Environ. Int.*, 2017, **102**, 165–176.

54 M. M. Borges-Ramírez, E. F. Mendoza-Franco, G. Escalona-Segura and J. Rendón-von Osten, *Environ. Pollut.*, 2020, **267**, 115659.

55 N. P. Ivleva, A. C. Wiesheu and R. Niessner, *Angew. Chem., Int. Ed.*, 2017, **56**, 1720–1739.

56 A. C. Silva, A. J. Silvestre, C. Vilela and C. S. Freire, *Molecules*, 2021, **27**, 94.

57 D. Ayre, *Curr. Opin. Green Sustainable Chem.*, 2018, **13**, 108–112.

58 E. Matei, A. M. Predescu, M. Râpă, A. A. □urcanu, I. Mateş, N. Constantin and C. Predescu, *Nanomaterials*, 2022, **12**, 1707.

59 C. J. C. Yann Bouchery, J. C. Fransoo and T. Tan, *Sustainable Supply Chains - A Research-Based Textbook on Operations and Strategy*, Springer, Cham, 1st edn, 2017.

60 Q. Chen, Y. Qi, Y. Jiang, W. Quan, H. Luo, K. Wu, S. Li and Q. Ouyang, *Mar. Drugs*, 2022, **20**, 536.

61 A. Apriyanto, J. Compart and J. Fettke, *Plant Sci.*, 2022, 111223.

62 P. Muthukumaran, P. Suresh Babu, S. Karthikeyan, M. Kamaraj and J. Aravind, *Int. J. Environ. Sci. Technol.*, 2021, **18**, 2491–2510.

63 G. Alberti, C. Zanoni, V. Losi, L. R. Magnaghi and R. Biesuz, *Chemosensors*, 2021, **9**, 108.

64 R. Brito-Pereira, A. S. Macedo, C. Ribeiro, V. F. Cardoso and S. Lanceros-Méndez, *Appl. Mater. Today*, 2022, **28**, 101507.

65 A. Reizabal, C. M. Costa, L. Pérez-Álvarez, J. L. Vilas-Vilela and S. Lanceros-Méndez, *Adv. Funct. Mater.*, 2023, **33**, 2210764.

66 A. Reizabal, C. Costa, L. Pérez-Álvarez, J. Vilas-Vilela and S. Lanceros-Méndez, *Polym. Rev.*, 2023, **63**, 1014–1077.

67 T. P. Nguyen, Q. V. Nguyen, V.-H. Nguyen, T.-H. Le, V. Q. N. Huynh, D.-V. N. Vo, Q. T. Trinh, S. Y. Kim and Q. V. Le, *Polymers*, 2019, **11**, 1933.

68 C. Narita, Y. Okahisa, I. Wataoka and K. Yamada, *ACS omega*, 2020, **5**, 22786–22792.

69 D.-L. Wen, D.-H. Sun, P. Huang, W. Huang, M. Su, Y. Wang, M.-D. Han, B. Kim, J. Brugger and H.-X. Zhang, *Microsyst. Nanoeng.*, 2021, **7**, 1–25.

70 D. T. Pham, N. Saelim and W. Tiyaboonchai, *J. Mater. Sci.*, 2018, **53**, 14087–14103.

71 R. F. Pereira, R. Brito-Pereira, R. Gonçalves, M. P. Silva, C. M. Costa, M. M. Silva, V. n. de Zea Bermudez and S. Lanceros-Méndez, *ACS Appl. Mater. Interfaces*, 2018, **10**, 5385–5394.

72 D. Terada, Y. Yokoyama, S. Hattori, H. Kobayashi and Y. Tamada, *Mater. Sci. Eng. C*, 2016, **58**, 119–126.

73 L.-P. Yan, J. M. Oliveira, A. L. Oliveira, S. G. Caridade, J. F. Mano and R. L. Reis, *Acta Biomater.*, 2012, **8**, 289–301.

74 A. Alessandrino, B. Marelli, C. Arosio, S. Fare, M. C. Tanzi and G. Freddi, *Eng. Life Sci.*, 2008, **8**, 219–225.

75 W. Zhou, H. Huang, S. Du, Y. Huo, J. He and S. Cui, *Appl. Surf. Sci.*, 2015, **345**, 169–174.

76 H. Wang, L. Liang, X. Cheng, Y. Luo and S. Sun, *Photochem. Photobiol.*, 2018, **94**, 17–26.

77 J. Zhou, Y. Zhang, Y. Yang, Z. Chen, G. Jia and L. Zhang, *Appl. Surf. Sci.*, 2019, **497**, 143762.

78 I. Garrido, S. Aznar-Cervantes, M. Aliste, M. J. Yáñez-Gascón, N. Vela, J. L. Cenis, S. Navarro and J. Fenoll, *Catalysts*, 2020, **10**, 110.

79 C. S. Ki, E. H. Gang, I. C. Um and Y. H. Park, *J. Membr. Sci.*, 2007, **302**, 20–26.

80 B. Milićević, V. Doradević, D. Lončarević, S. P. Ahrenkiel, M. D. Dramićanin and J. M. Nedeljković, *Microporous Mesoporous Mater.*, 2015, **217**(C7–7187), 184–189.

81 V. Lazić, I. Smičiklas, J. Marković, D. Lončarević, J. Dostanić, S. P. Ahrenkiel and J. M. Nedeljković, *Vacuum*, 2018, **148**, 62–68.

82 A. Reizabal, S. Gonçalves, R. Brito-Pereira, P. Costa, C. M. Costa, L. Pérez-Álvarez, J. L. Vilas-Vilela and S. Lanceros-Méndez, *Nanoscale Adv.*, 2019, **1**, 2284–2292.

83 H. Salazar, P. M. Martins, M. M. Fernandes, P. Costa, S. Ferdov, G. Botelho and S. Lanceros-Mendez, *J. Hazard. Mater.*, 2022, **440**, 129756.

84 H. Yang, S. Yang, J. Kong, A. Dong and S. Yu, *Nat. Protoc.*, 2015, **10**, 382–396.

85 P. Martins, A. C. Lopes and S. Lanceros-Mendez, *Prog. Polym. Sci.*, 2014, **39**, 683–706.

86 R. E. Sousa, J. Nunes-Pereira, J. C. C. Ferreira, C. M. Costa, A. V. Machado, M. M. Silva and S. Lanceros-Mendez, *Polym. Test.*, 2014, **40**, 245–255.

87 S. S. Abdullahi, S. Güner, Y. Musa, B. I. Adamu and M. I. Abdulhamid, *NAMP J*, 2016, **35**, 241–246.

88 D. K. Božanić, G. A. Garcia, L. Nahon, D. Sredojević, V. Lazić, I. Vukoje, S. P. Ahrenkiel, V. Djoković, Ž. Šljivančanin and J. M. Nedeljković, *J. Phys. Chem. C*, 2019, **123**, 29057–29066.

89 D. A. O, A. Olalekan, A. Olatunya and A. O. Dada, *J. Appl. Chem.*, 2012, **3**, 38–45.

90 R. Brito-Pereira, D. Correia, C. Ribeiro, A. Francesko, I. Etxebarria, L. Pérez-Álvarez, J. Vilas, P. Martins and S. Lanceros-Mendez, *Composites, Part B*, 2018, **141**, 70–75.

91 E. O. Carvalho, M. Rincón-Iglesias, R. Brito-Pereira, E. Lizundia, M. M. Fernandes and S. Lanceros-Mendez, *Int. J. Biol. Macromol.*, 2023, **242**, 125049.

92 P. M. Martins, R. Miranda, J. Marques, C. J. Tavares, G. Botelho and S. Lanceros-Mendez, *RSC Adv.*, 2016, **6**, 12708–12716.

93 A. Reizabal, N. Castro, N. Pereira, C. M. Costa, L. Pérez, J. L. Vilas-Vilela and S. Lanceros-Méndez, *ACS Appl. Electron. Mater.*, 2022, **4**, 1901–1909.

94 Z. Shao, F. Vollrath, J. Sirichaisit and R. J. Young, *Polymer*, 1999, **40**, 2493–2500.

95 P. Martins, C. Caparros, R. Gonçalves, P. Martins, M. Benelmekki, G. Botelho and S. Lanceros-Mendez, *J. Phys. Chem. C*, 2012, **116**, 15790–15794.

96 A. Reizabal, R. Brito-Pereira, M. M. Fernandes, N. Castro, V. Correia, C. Ribeiro, C. M. Costa, L. Perez, J. L. Vilas and S. Lanceros-Méndez, *Materialia*, 2020, **12**, 100709.

97 M. K. Sah and K. Pramanik, *Afr. J. Biotechnol.*, 2011, **10**, 7878–7892.

98 Y. Kim and B. Park, *Mater. Lett.*, 2022, **316**, 132001.

99 C. H. Nguyen, T. T. V. Tran, M. L. Tran and R.-S. Juang, *J. Taiwan Inst. Chem. Eng.*, 2023, **145**, 104825.

100 J.-S. Choi, S. Kim, Y. Choi, K. B. Kim, H.-J. Kim, T. J. Park and Y. M. Park, *Surf. Interfaces*, 2022, **34**, 102380.

101 M. M. Momeni, M. Mirhosseini and N. Mohammadi, *J. Mater. Sci.: Mater. Electron.*, 2016, **27**, 6542–6551.

102 L. Lin, H. Wang, W. Jiang, A. R. Mkaouar and P. Xu, *J. Hazard. Mater.*, 2017, **333**, 162–168.

103 S. Teixeira, B. Magalhães, P. M. Martins, K. Kühn, L. Soler, S. Lanceros-Méndez and G. Cuniberti, *Global Challenges*, 2018, **2**, 1700124.

104 N. Malesic-Eleftheriadou, E. N. Evgenidou, G. Z. Kyzas, D. N. Bikiaris and D. A. Lambropoulou, *Chemosphere*, 2019, **234**, 746–755.

105 A. K. Yontar, S. Avcioğlu and S. Çevik, *J. Cleaner Prod.*, 2022, **380**, 135070.

106 N. Ali, Awais, T. Kamal, M. Ul-Islam, A. Khan, S. J. Shah and A. Zada, *Int. J. Biol. Macromol.*, 2018, **111**, 832–838.

107 S. Elbakry, M. E. A. Ali, M. Abouelfadl, N. A. Badway and K. M. M. Salam, *J. Photochem. Photobiol., A*, 2022, **430**, 113957.

108 M. M. Momeni, Y. Ghayeb and S. Gheibee, *Ceram. Int.*, 2017, **43**, 564–570.

109 H. Zhou, X. Wang, T. Wang, J. Zeng, Z. Yuan, J. Jian, Z. Zhou, L. Zeng and H. Yang, *Eur. Polym. J.*, 2019, **118**, 153–162.

110 S. Teixeira, P. Martins, S. Lanceros-Méndez, K. Kühn and G. Cuniberti, *Appl. Surf. Sci.*, 2016, **384**, 497–504.

111 T. Navab-Daneshmand, M. N. Friedrich, M. Gächter, M. C. Montealegre, L. S. Mlambo, T. Nhiwatiwa, H.-J. Mosler and T. R. Julian, *Am. J. Trop. Med. Hyg.*, 2018, **98**, 803.

112 W. Sim, R. T. Barnard, M. A. T. Blaskovich and Z. M. Ziora, *Antibiotics*, 2018, **7**, 93.

113 C. N. Paiva and M. T. Bozza, *Antioxid. Redox Signaling*, 2014, **20**, 1000–1037.

114 M. M. Fernandes, E. O. Carvalho, D. M. Correia, J. M. Esperança, J. Padrão, K. Ivanova, J. Hoyo, T. Tzanov and S. Lanceros-Mendez, *ACS Appl. Bio Mater.*, 2022, **5**, 5181–5189.

115 T. D. Tavares, J. C. Antunes, J. Padrão, A. I. Ribeiro, A. Zille, M. T. P. Amorim, F. Ferreira and H. P. Felgueiras, *Antibiotics*, 2020, **9**, 314.

116 T. A. Seregina, I. Y. Petrushanko, R. S. Shakulov, P. I. Zaripov, A. A. Makarov, V. A. Mitkevich and A. S. Mironov, *Cells*, 2022, **11**, 2667.